Int. J. Environ. Res., 8(4):1171-1184, Autumn 2014
ISSN: 1735-6865

Development of NiO-Co_3O_4 nano-ceramic composite materials as novel photocatalysts to degrade organic contaminants present in water

Mohamed Jaffer Sadiq, M.[1] and Samson Nesaraj, A.[2*]

[1]Department of Nanosciences and Technology, Karunya University, Coimbatore - 641 114, India

[2]Department of Chemistry, Karunya University,Coimbatore – 641 114, India

Received 7 March 2014; Revised 29 May 2014; Accepted 2 June 2014

ABSTRACT: Novel ceramic oxides have been increasingly focused in recent years because of their potential applications in environmental purification especially to treat organic contaminants present in water. In this research work, a set of NiO-Co_3O_4 nano-ceramic composite materials were prepared by a simple reflux condensation method using nickel acetate / cobalt acetate as precursor salts, sodium monododecyl sulphate (SDS) as a surfactant and N,N-Dimethylformamide (DMF) as solvent. The prepared nano-ceramic composites were calcined at different temperatures such as 200, 400, 600 and 800°C for 2 hours each to get the phase pure product. XRD results revealed that all the samples indexed to a cubic crystalline geometry. The presence of metal-oxygen bond (Ni-O and Co-O) was confirmed by FTIR spectroscopy. The presence of Ni, Co and O in the sample was confirmed by EDAX analysis. The existence of particles in nanometer range was shown by SEM. The particle size analysis by light scattering method also confirmed the particles in nanometer range (approximately 270 nm) in all the three samples. The optical behavior of the materials was studied by UV-Vis and PL spectrophotometer. Photocatalytic activity studies carried out with NiO-Co_3O_4 (1.0:1.0) nano-ceramic composites in presence of organic dyes such as, rhodamine B and methyl orange dyes under UV light irradiation (for two hours) resulted in the degradation of 77% and 84% respectively.

Key words: NiO-Co_3O_4 nano-ceramic, Reflux, Photocatalytic, Degradation, Organic, Dyes, Water

INTRODUCTION

Adequate purification of industrial waste water is a major concern because it may contain hazardous pollutants. Hence, novel waste water treatment technologies are needed to save the environment from pollution. Because of the growth of textile and leather industries, huge amount of toxic waste water is released everyday into the aqueous ecosystem (Park *et al.,* 2003). The polluted waste water contains of variety of pollutants with high concentration and complicated composition. The removal of organic compounds in the industrial waste water is a major concern in ensuring a safe and healthy environment (Gao *et al.,* 2011). It was found that the semiconductor photocatalysts can easily degrade the organic pollutants present in industrial waste water under UV/solar light or visible light irradiation (Kanjwal *et al.,* 2010). Recently, nanostructured transition metal oxide materials were also proposed as effective photocatalysts (Teo *et al.,* 2006). The oxide materials such as, nickel oxide and cobalt oxide are the versatile materials from the transition-metal oxides for any application in normal environment condition (Zav'yalova, *et al.,* 2007). NiO is a p-type semiconductor and wide band gap energy range from 3.4 - 4 eV (Sasi *et al.,* 2007). NiO is studied various groups since it has an excellent durability and electrochemical stability as well due to its good optical, magnetic and electrical characteristics (Bandara *et al.,* 2007). Cobalt oxide is also a p-type semiconductor and it is having a direct energy band gap at 1.5 - 2.0 eV (Wang *et al.,* 2009). It is a spinel crystal structure (Fd3m) and also has excellent magnetic, optical and transport properties (Yamamoto *et al.,* 2002). Both nickel oxide and cobalt oxide were utilized in the diversified areas of industry such as electronic devices (Romana *et al.,* 2006), catalysts (Warang *et al.,* 2012), battery (Lou *et al.,* 2008), dye-sensitized solar cell devices (Taniguchi *et al.,* 2001), gas sensor (Li *et al.,* 2005), super capacitors (Co *et al.,* 2005), antiferro magnetic materials (Nethravathi *et al.,* 2005), solar cells (Irwin *et al.,* 2008), fuel cell electrodes (Kim *et al.,* 2004), sensors (Varghese *et al.,* 2008) and in other advanced

*Corresponding author E-mail: drsamson@karunya.edu

applications also (Kalu *et al.,* 2001; Nam *et al.,* 2002). Recently, several methods have been developed for the preparation of nickel oxide and cobalt oxide by different routes such as, thermal decomposition (Wang *et al.,* 2005), solvothermal (Beach *et al.,* 2009), sol-gel (Park *et al.,* 2004), chemical method (Yang *et al.,* 2008), co precipitation (Xin *et al.,* 2007), micro emulsion (Han *et al.,* 2004), spray pyrolysis (Puspharajah *et al.,* 1997), hydrothermal method (Chen *et al.,* 2005) and by other means also (Parada *et al.,* 2006; Morsy *et al.,* 2009). It was reported that the composite materials can be effectively utilized for photocatalytic applications. The composite materials such as, NiO-SiO_2 (Singhal *et al.,* 2008), TiO_2-SiO_2 (Schneider *et al.,* 2001), CdS-TiO_2 (So *et al.,* 2004), ZnS-TiO_2 (Yu *et al.,* 2006), CuO-TiO_2 (Xu *et al.,* 2009), WO_3-SiCeTiO_2 (Keller *et al.,* 2003), $SrTiO_3$-TiO_2 (Yan *et al.,* 2009), SnO_2-TiO_2 (Sasikala *et al.,* 2009), ZnO-SnO_2 (Asokan *et al.,* 2010), ZnO-TiO_2 (Yang *et al.,* 2009), ZnO-In_2O_3 (Wang *et al.,* 2009), NiO-ZnO (Hameed *et al.,* 2009), ZnO–ZnS (Lahiri *et al.,* 2009) and NiO–WO_3 (Na *et al.,* 2005) were reported and studied for photocatalytic applications. The photocatalytic degradation of organic dyes such as methyl blue, methyl orange, rhodamine B and phenol was studied by several groups (Chen *et al.,* 2008; Abu-Zied *et al.,* 2008). In this research paper, we report the preparation and characterization of set of NiO-Co_3O_4 nano-ceramic composites by a simple reflux condensation method and report their photocatalytic characteristics in degrading the organic dyes such as rhodamine B and methyl orange present in water.

MATERIALS & METHODS

All the chemicals are analytical in grade such as Nickel (II) acetate tetra hydrate (98.0% purity, Merck, India), Cobalt (II) acetate tetra hydrate (98.0% purity, Sigma-Aldrich, India), N, N-Dimethylformamide (99.8% purity, Merck, India), sodium mono dodecyl sulphate (> 99% purity, Merck, India), Methyl Orange (>98.0% purity, Merck, India), Rhodamine B (>95.0% purity, Sigma-Aldrich, India) and Ethanol (99.0% purity, Merck, India). All the received chemicals were used as without any further purification. All the reactions were carried out by using deionized water.

NiO-Co_3O_4 nano-ceramic composites (with three reactant mole ratios such as 1.5:0.5, 1.0:1.0, 0.5:1.5) were prepared by reflux condensation method. In the typical

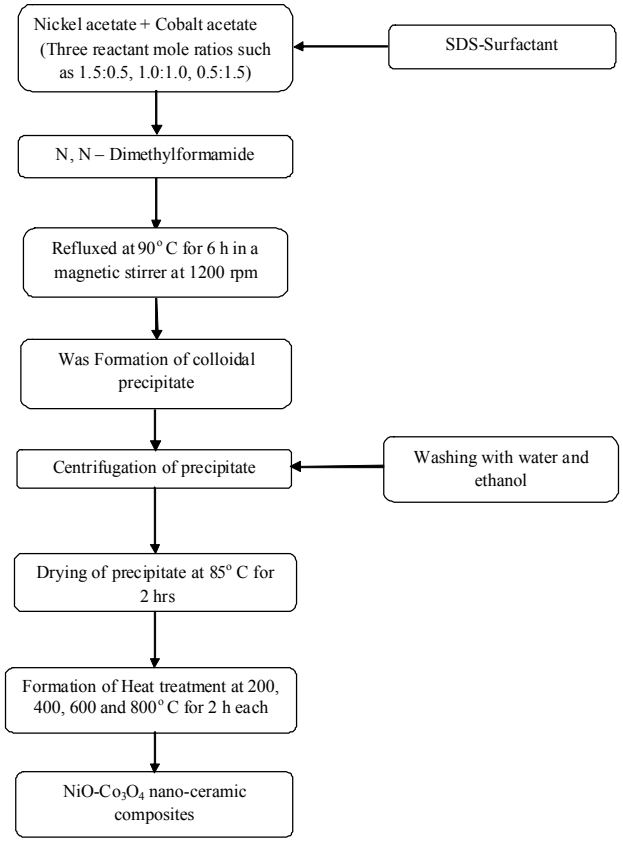

Fig. 1. Flow chart to prepare NiO-Co_3O_4 nano-ceramic composites by reflux condensation method

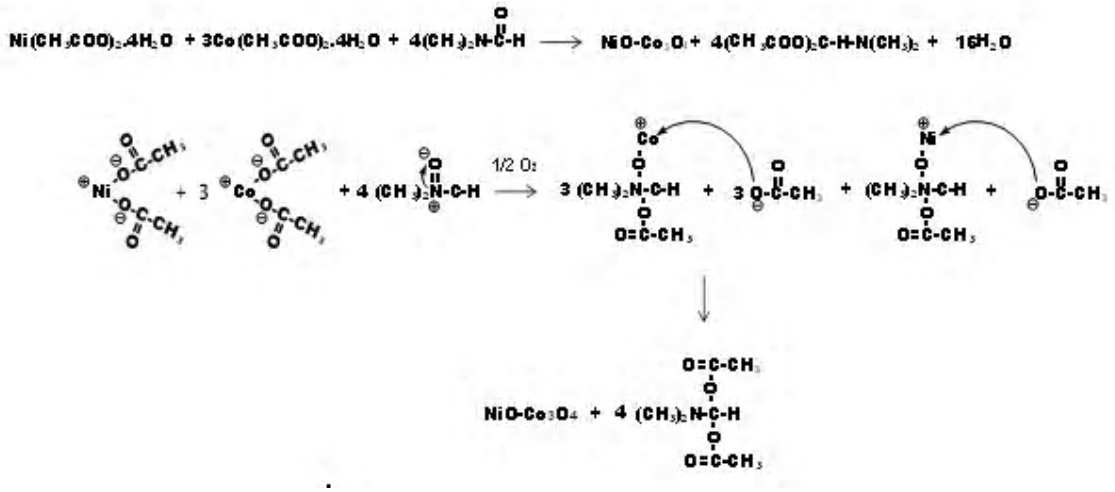

Fig. 2. Reaction mechanism involved in the synthesis of NiO-Co_3O_4 nano-ceramic composite material

experiment, calculated amount of metal acetate salts were dissolved in DMF solution (100 ml each) with 1 % SDS as surfactant. The above solution mixture was stirred (1200 RPM) at room temperature for about 10 minutes followed by refluxing at 90°C for 6 hrs. A colloidal precipitate was obtained. The resultant colloidal precipitate was centrifuged and washed with 10% ethanol. The products were dried at 85°C for 2 hours. Finally, the dried products were calcined at different temperatures with 200, 400, 600 and 800 °C for each 2 hours. The flow chart of the synthesized NiO-Co_3O_4 nano-ceramic composites is indicated in Fig. 1. The reaction mechanism involved in the synthesis of NiO-Co_3O_4 nano-ceramic composite material is indicated in Fig.2

The structural characterization were carried out with powder X-ray Diffractometer system (XRD Lab X Shimadzu) using CuKα radiation (λ = 0.154059 nm) with a nickel filter in the 2θ scanning ranges from 30° to 90° with a scan rate at 10°/min. The applied voltage and current were 40 kV and 30 mA respectively. The crystalline sizes were calculated by using the Debye-Scherrer formula. The chemical structure were recorded by Fourier transform infrared spectra (SHIMADZU Spectrophotometer) using KBr pellet technique in the range from 4000/cm to 400/cm (spectral resolution at 4/cm and number of scans at 20). The average particle sizes were measured with a Zetasizer Ver. 6.32 manufactured by the Malvern Instruments Ltd, UK. The sample (0.01g) was well dispersed in water (20ml) around 30 min before carrying out the particle size analysis. The surface morphology, size of particles and elemental compositions were carried out by scanning electron microscope (SEM JEOL JSM-6610) well equipped with an energy dispersive X-ray (EDAX) spectrophotometer and operated at 20kV. Absorbance spectrum were recorded by using UV-Vis spectroscopy (JASCO V-60 spectrophotometer) at range between 200-600nm. Photoluminescence spectrums were measured by spectroflurophotometer (FLUOROLOG, HORIBA YVON) with Xe laser as the excitation light source at room temperature.

In this comparative study, the dyes such as, rhodamine B (RB) and methyl orange (MO) were used in the investigation of photocatalytic characteristics of the as-prepared NiO-Co_3O_4 (with three reactant mole ratios such as 1.5:0.5, 1.0:1.0, 0.5:1.5) nano-ceramic composite materials. The photocatalytic degradation of dyes such as, rhodamine B and methyl orange in the presence of pure NiO-Co_3O_4 (with three reactant mole ratios such as 1.5:0.5, 1.0:1.0, 0.5:1.5) nano-ceramic composites as well as in the absence of NiO-Co_3O_4 nano-ceramic composites were carried out in a simple Pyrex photoreactor. The dyes (both rhodamine B and methyl orange) with concentration of 1.0×10^{-5}M were used in the present study. In each experiment, 10 mg of the prepared photocatalyst (NiO-Co_3O_4 nano-ceramic composite material) was mixed with 50 ml of above dye solution and then sonicated for about 10 minutes in a sonicator. The above reaction mixture was loaded in the photoreactor and again stirred well for about 30 minutes in dark to attain adsorption equilibrium condition. After this process, the reaction mixture was exposed to UV light under continuous stirring and the corresponding optical density values of the reaction mixture was recorded at time intervals such as, 0, 30, 60, 90 and 120 minutes. The absorbance studies for rhodamine B and methyl orange dye solutions were carried out at the wavelength of 554 and 465 nm respectively.

RESULTS & DISCUSSION

The powder XRD patterns of as-synthesized NiO-Co_3O_4 nano-ceramic composites are indicated in Fig. 3. The XRD pattern displays in the 2θ range between 30˝ to 90˝. The NiO peaks found at (111), (200), (220), (311) and (222) in all the three samples were matched well with the standard reported values (JCPDS) for NiO indexed in JCPDS No. 01-1239. The Co_3O_4 peaks found at (220), (311), (222), (400), (422), (511), (440), (533) and (444) in all the three samples were matched well with the standard data for Co_3O_4 (JCPDS pattern No. 65-3103). The diffraction peaks found in all the samples can be exactly indexed to a cubic crystalline geometry. No impurity peaks were observed in the samples. The lattice parameters values were measured from 2θ values in the XRD patterns are indicated in the Table 1.

The crystal sizes (D) were calculated by using the Debye-Scherrer formula (Sapra *et al.*, 2005) from equation (1).

$$D = 0.91\,\lambda / \beta \cos\theta \quad (1)$$

Where 'λ' is the X-ray source wavelength (λ =0.1540 nm for CuKα), 'β' is the F_{WHM} (full width at half maximum) and 'θ' is the Bragg's angle at the X-ray source.

The theoretical densities (Dx) (Rao, 1963) were calculated from equation (2).

$$Dx = (Z * M) / (N * a^3)\ g.cm^{-3} \quad (2)$$

Where 'Z' is the number of chemical species present in the unit cell, 'M' is the molecular mass of the sample (g/mol), 'N' is the Avogadro's number (6.023×10^{23}) and 'a' is the lattice constant (cm) calculated from equation (3).

The lattice constant (Xu and Zeng, 1998) of the cubic system were calculated from the equation (3).

$$a = d * (h^2 + k^2 + l^2)^{1/2} \quad (3)$$

Table 1. The crystallographic parameters obtained on were obtained on NiO-Co_3O_4 nano-ceramic composites

Sample	Crystal structure	Unit cell lattice parameter 'a' (Å)	Unit cell volume $(Å)^3$	Theoretical density (g/cc)	Crystallite size (nm)
Standard XRD data for NiO powder (JCPDS No. 01-1239)	Cubic	4.1568	71.8253	6.9070	--
Standard XRD data for Co_3O_4 powder (JCPDS No. 65-3103)	Cubic	8.047	521.0771	6.1381	--
NiO- Co_3O_4 (1.5 : 0.5)	Cubic	4.2107	74.6557	8.4199	3.6281
NiO- Co_3O_4 (1.0 : 1.0)	Cubic	4.1640	72.1992	8.706	2.4796
NiO- Co_3O_4 (0.5 : 1.5)	Cubic	5.5063	166.9474	3.7616	4.6203

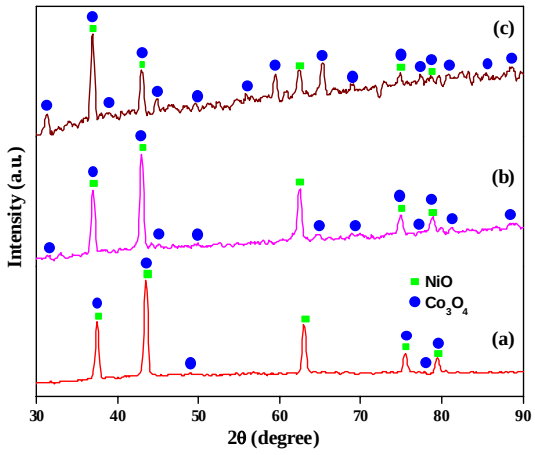

Fig. 3. The XRD pattern of NiO-Co_3O_4 nano-ceramic composites for different reactant mole ratios (a) 1.5:0.5, (b) 1.0:1.0 and (c) 0.5:1.5

The FT-IR spectra of as-synthesized NiO-Co_3O_4 nano-ceramic composites are indicated in Fig. 4. FTIR studies were carried out to understand the presence of functional group of any organic molecule. In the investigated region (4000-400 cm^{-1}), it showed significant absorption peaks at 3700-3800, 2890, 2360, 1700, 1500, 1100, 665, 569, 465 and 420/cm. It is noted that the bands at approximately 3700-3800 and 1700, 1500, 1100 cm^{-1} were assigned to the stretching and bending vibrations of the water molecules (Pejova *et al.*, 2001). Also, there is a band at approximately 2890 and 2360 cm^{-1} which may be assigned due to the presence of C–H symmetric stretching mode on the surface (Xing *et al.*, 2004). Generally any metal oxides absorption bands below 1000/cm arising from inter-atomic vibrations (Sun *et al.*, 2009). The presence of two absorption bands at 569 and 665/cm was assigned to Co-O stretching vibration (Co^{3+} in the octahedral hole) mode and bridging vibration of O-Co-O bond (Co^{2+} in the tetrahedral hole) which originate from the stretching vibrations of the metal-oxygen bond and confirm the formation of Co_3O_4 spinel oxide (Venkatnarayan *et al.*, 2006). The broad absorption band in the region of 420-465/cm is assigned to Ni-O stretching vibration mode (Gnanachari *et al.*, 2012).

The particle size distribution curve of NiO-Co_3O_4 nano-ceramic composites is shown in Fig. 5. The particle size histograms obtained on NiO-Co_3O_4 nano-ceramic composites possessed narrow particle size distribution patterns and the mean particle diameter are indicated in the Table 2. The mean particle size determined by particle size analyzer is very close to the average particle size calculated by the SEM. The

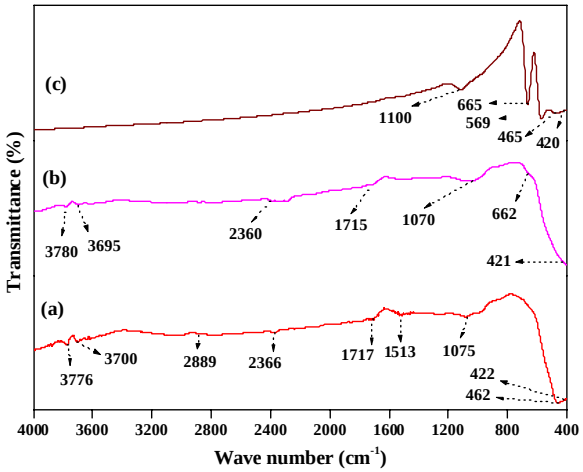

Fig. 4. The FTIR spectra of NiO-Co_3O_4 nano-ceramic composites for different reactant mole ratios (a) 1.5:0.5, (b) 1.0:1.0 and (c) 0.5:1.5

Table 2. The particle characteristics of NiO-Co_3O_4 nano-ceramic composites

Sample		Peak 1		Peak2		Average particle size (nm)
		Intensity (%)	Diameter (nm)	Intensity (%)	Diameter (nm)	
	1.5:0.5	100	277.5	0	0	274.9
	1:1	98.1	323.3	1.9	64.13	273.6
NiO-Co_3O_4	0.5:1.5	100	321.7	0	0	280.7

Table 3. The EDAX data obtained on NiO-Co_3O_4 nano-ceramic composites

Sample		Atomic Weight percentage of elements		
		Ni	Co	O
	1.5:0.5	21.60	6.64	71.76
	1:1	18.87	10.61	70.51
NiO-Co_3O_4	0.5:1.5	9.34	21.76	68.90

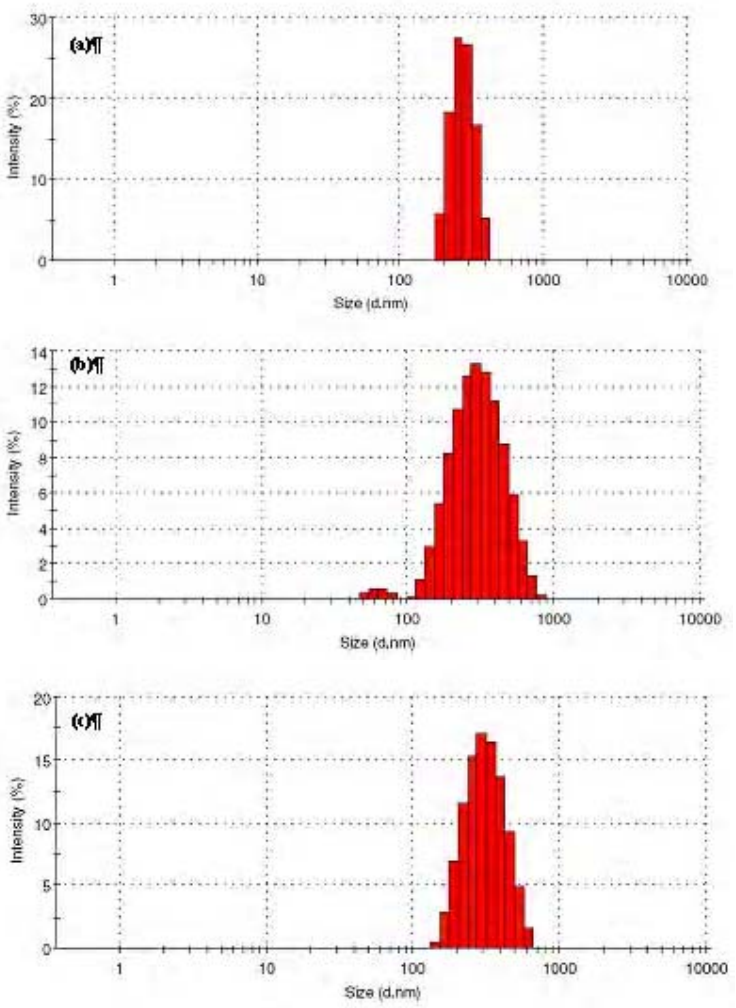

Fig. 5. The particle size distribution of NiO-Co_3O_4 nano-ceramic composites for different reactant mole ratios (a) 1.5:0.5, (b) 1.0:1.0 and (c) 0.5:1.5

large particle size observed in the particles may be due to the agglomeration of particles observed at high temperature treatment (Lee, 2001).

The SEM images of NiO-Co_3O_4 nano-ceramic composites are shown in Fig. 6. It can be seen that the grain size of the particles present in the range of 200-300 nm in all the samples. In addition, spherical shaped grains were also present. The presence of aggregation in the samples may be due to the occurrence of large surface energy and surface tension because of high temperature treatment (Hongve and Akeson, 1996). The EDAX spectra of NiO-Co_3O_4 nano-ceramic composites are shown in Fig. 7. The presence of Ni, Co and O in the sample was confirmed by EDAX analysis. The chemical composition data of as-synthesized NiO-Co_3O_4 nano-ceramic composites are indicated in Table 3. The variation in the percentage of elements (Ni, Co and O) may be due to the reaction conditions during the preparation of NiO-Co_3O_4 nano-ceramic composites.

The optical absorption spectra of NiO-Co_3O_4 nano-ceramic composites are shown in Fig. 8. From the absorption spectra, it was found that the wavelength was observed at 256.5, 256 and 257 nm for the samples (1.5:0.5, 1.0:1.0, 0.5:1.5 reactant mole ratios). The absorption energy band gap (Eg) can be determined by the following Tauc (Devi *et al.*, 2007) equation (4)

$$(Ahv)^n = K (hv - Eg) \quad (4)$$

Where, hν is the photon energy (eV), A is the absorption coefficient, K is a constant relative to the material, Eg is the band gap and n is either 1/2 for an indirect transition or 2 for a direct transition. The direct band gap can be estimated by extrapolating the linear

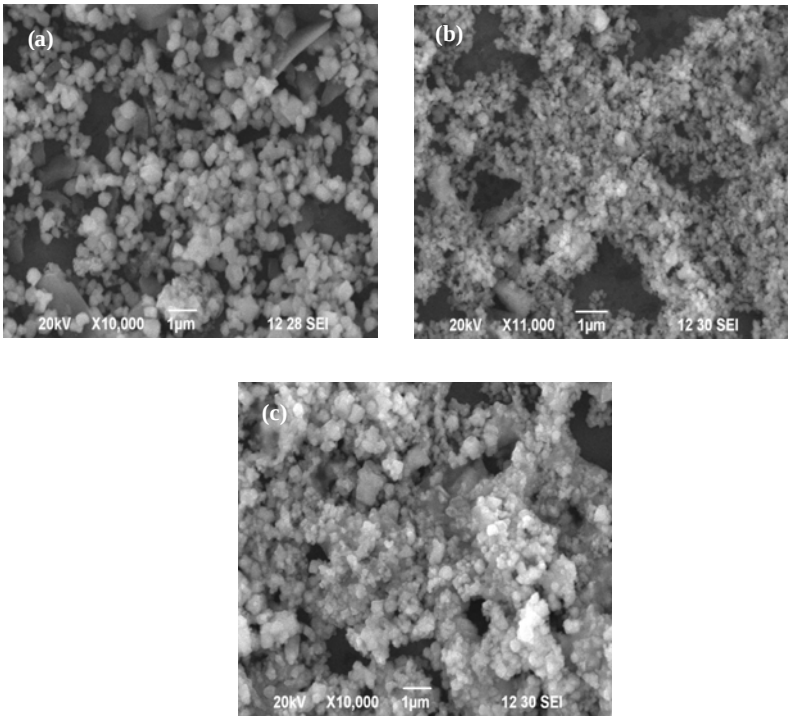

Fig. 6. The SEM images of NiO-Co_3O_4 nano-ceramic composites for different reactant mole ratios (a) 1.5:0.5, (b) 1.0:1.0 and (c) 0.5:1.5

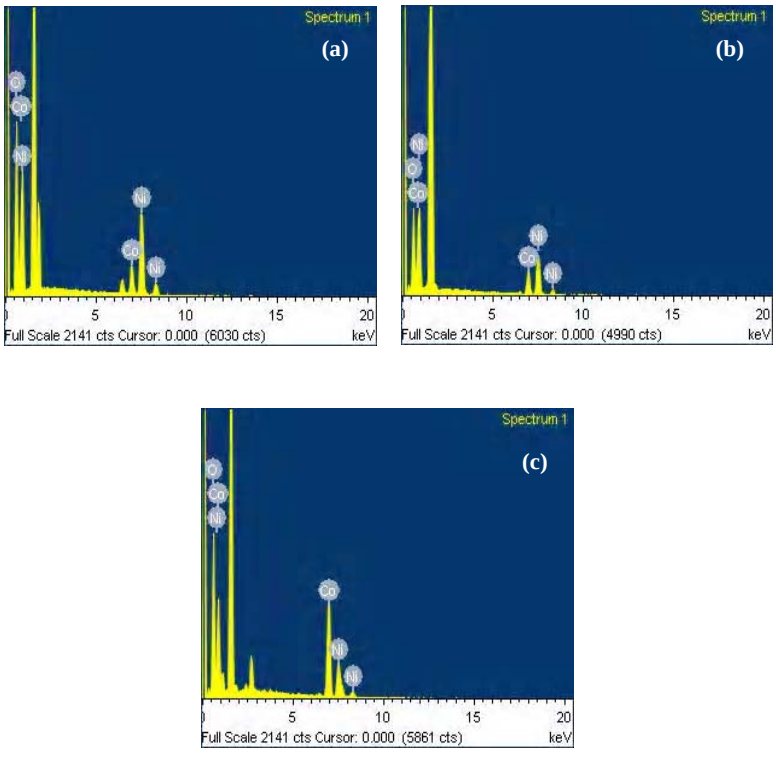

Fig. 7. The EDAX spectra of NiO-Co_3O_4 nano-ceramic composites for different reactant mole ratios (a) 1.5:0.5, (b) 1.0:1.0 and (c) 0.5:1.5

region in the Tauc plot of $(Ahv)^2$ versus photon energy (hv) as shown in the Fig. 9. This gives the energy band gap values of NiO-Co_3O_4 nano-ceramic composites as 5.75, 5.84, 5.72 eV respectively. The reported band gap value (Ai and Jiang, 2009), the Eg values of as-synthesized NiO-Co_3O_4 nano-ceramic composites are greater than those of bulk NiO and Co_3O_4 (3.4-4.0 eV and 1.77-3.17 eV respectively). The increase in the band gap value of NiO-Co_3O_4 nano-ceramic composites may be due to the quantum confinement effects of the nanoparticles (Zhang *et al.*, 2007). The PL Emission spectra of NiO-Co_3O_4 nano-ceramic composites are shown in Fig. 10. According to the wavelength of UV absorbance spectra, the nanoc-ceramic composites exhibited the excitation wavelength at 270 nm. Strong broad emission peaks were found for the NiO-Co_3O_4 nano-ceramic composites at 308, 307 and 309 nm respectively. The strong broad emission peaks appeared in all the samples may be due to the high purity and perfect crystalline nature (Mohamed and Nesaraj, 2013). Fig. 11 shows the degradation percentage curve of rhodamine B in presence NiO-Co_3O_4 nano-ceramic

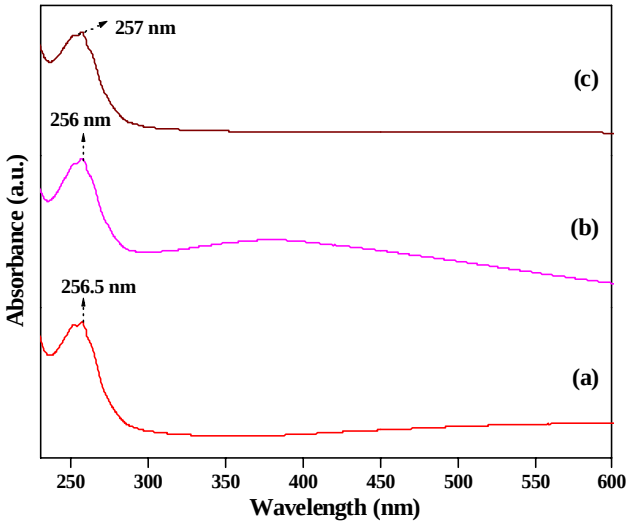

Fig. 8. Absorbance spectra of NiO-Co_3O_4 nano-ceramic composites for different reactant mole ratios (a) 1.5:0.5, (b) 1.0:1.0 and (c) 0.5:1.5

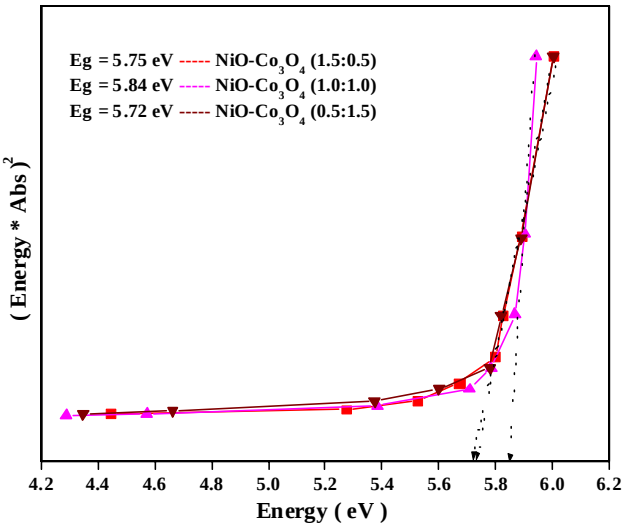

Fig. 9. Energy band gap spectra of NiO-Co_3O_4 nano-ceramic composites for different reactant mole ratios (a) 1.5:0.5, (b) 1.0:1.0 and (c) 0.5:1.5

composites irradiated under UV light. The degradation rate of rhodamine B dye without catalyst was found to be only 23 % even after 120 minutes exposure to UV light. However, in presence of NiO-Co_3O_4 (1.5:0.5, 1.0:1.0, 0.5:1.5) nano-ceramic composites, rhodamine B was degraded 69, 77 and 61 % respectively after exposure to UV radiation for about 120 minutes. Fig. 12 shows the degradation percentage curve of methyl orange in presence NiO-Co_3O_4 nano-ceramic composites irradiated under UV light. The degradation rate of methyl orange dye without catalyst was performed and it was found to be 18 % only even after 120 minutes of exposure to UV light. However, in presence of NiO-Co_3O_4 (1.5:0.5, 1.0:1.0, 0.5:1.5) nano-ceramic composites, methyl orange was degraded 56, 84 and 46 % respectively after exposure to UV radiation for about 120 minutes. Both the results have shown a good level of decrease in the absorption intensity with respect to time. From the result, it was found that sample with the composition, NiO-Co_3O_4 (1.0:1.0 mole reactant ration) has good photocatalytic characteristics in degrading the organic dyes such as, rhodamine B and methyl orange under UV light irradiation.

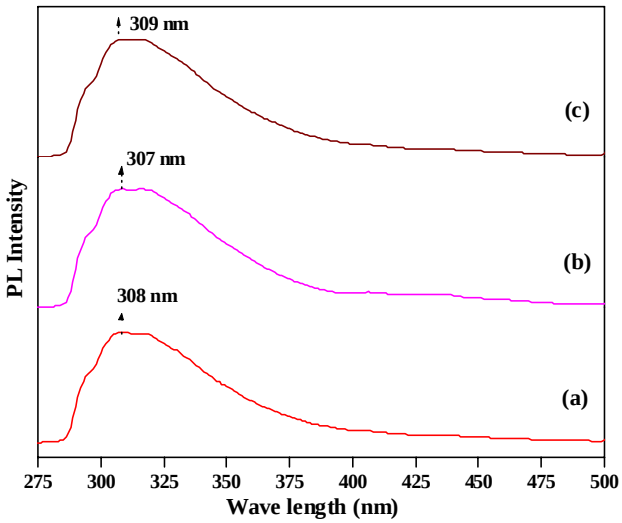

Fig. 10. Emission spectra of NiO-Co_3O_4 nano-ceramic composites for different reactant mole ratios (a) 1.5:0.5, (b) 1.0:1.0 and (c) 0.5:1.5

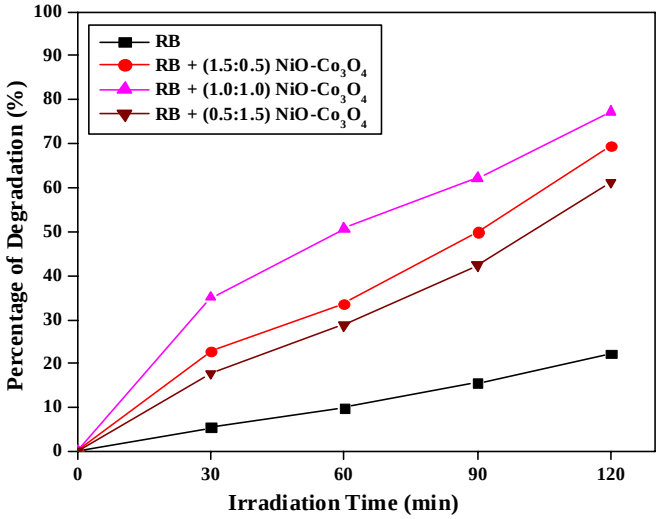

Fig. 11. Percentage degradation of Rhodamine B in the NiO-Co_3O_4 nano-ceramic composites for different reactant mole ratios (1.5:0.5, 1.0:1.0, 0.5:1.5)

The percentageof degradation wascalculated (Amaral *et al.*, 2004) from formula (5).

$$\text{The percentage of degradation} = ((C_0 \text{“ } C_t) / C_0) \times 100 \quad (5)$$

Where, C_0 is the initial absorbance of the dye solution and C_t is the absorbance at regular time interval respectively.

Photocatalytic reactions with different dye can be expressed by the Langmuir-Hinshelwood kinetics (Asiri *et al.*, 2011). The photocatalytic degradation of rhodamine B and methyl orange with/without photocatalysts under UV light obeys pseudo-first-order kinetics with respect to the degradation time and followed the liner equation (6).

$$\ln(c_0/c_t) = k_{app}t \quad (6)$$

Where, c_t and c_0 is the reactant concentrations at times t = t and t = 0, 'k_{app}' and 't' is the apparent reaction rate constant and interval time 'respectively.

The kinetics spectra (a plot of $\ln(c_0/c_t)$ versus UV light irradiation time t) of NiO-Co_3O_4 nano-ceramic composites in rhodamine B are shown in Fig. 13. The apparent first-order constant is determined as 0.00244, 0.00625 and 0.01157 (with NiO-Co_3O_4 nano-ceramic

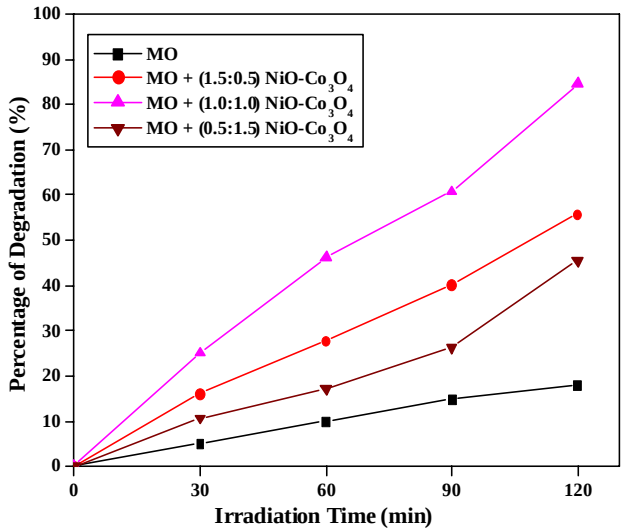

Fig. 12. Percentage degradation of Methyl Orange in the NiO-Co_3O_4 nano-ceramic composites for different reactant mole ratios (1.5:0.5, 1.0:1.0, 0.5:1.5)

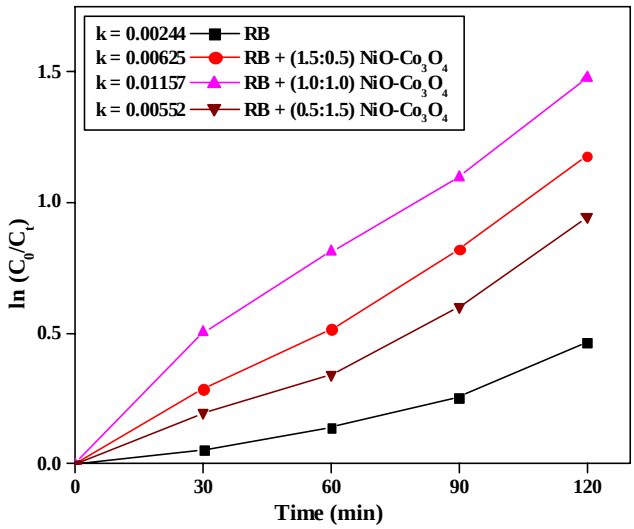

Fig. 13. Kinetics linear curves of Rhodamine B in the NiO-Co_3O_4 nano-ceramic composites for different reactant mole ratios (1.5:0.5, 1.0:1.0, 0.5:1.5)

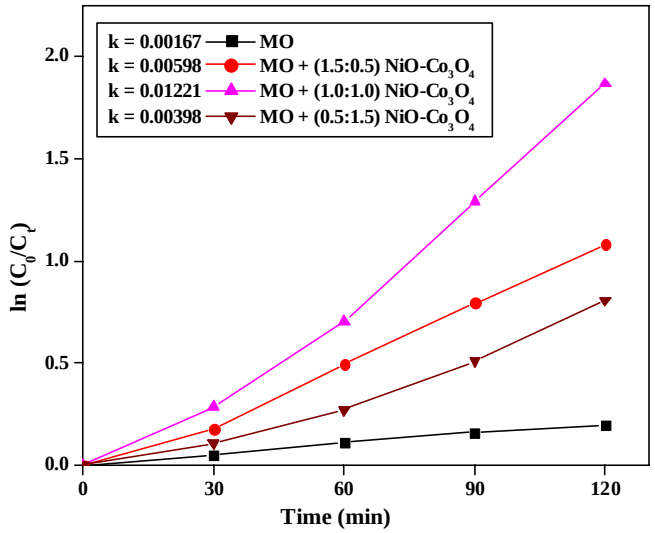

Fig. 14. Kinetics linear curves of Methyl Orange in the NiO-Co_3O_4 nano-ceramic composites for different reactant mole ratios (1.5:0.5, 1.0:1.0, 0.5:1.5)

composites) and 0.00552 (without catalysts). for rhodamine B. It was found that the reaction rate calculated for rhodamine B with 10 mg of NiO-Co_3O_4 (1.0:1.0) nano-ceramic composites was in good agreement with the results. The kinetics spectra of NiO-Co_3O_4 nano-ceramic composites in methyl orange are shown in Fig. 13. The apparent first-order constant is determined as 0.00167, 0.00598 and 0.01221 (with NiO-Co_3O_4 nano-ceramic composites) and 0.00398 (without catalysts) for methyl orange. The reaction rate calculated with methyl orange with 10mg of NiO-Co_3O_4 (1.0:1.0) nano-ceramic composites was in good agreement with the results. From the experimental results, it was confirmed that the NiO-Co_3O_4 (1.0:1.0) nano-ceramic composite is showing better photocatalytic characteristics in the photodegradation of rhodamine B (77 %) and methyl orange (84 %) dyes under UV light irradiation.

CONCLUSIONS

NiO-Co_3O_4 nano-ceramic composites were prepared by reflux condensation method using SDS as surfactant and the results are reported. The XRD data obtained on NiO-Co_3O_4 nano-ceramic composites shows that crystallized face-centered cubic in nature. The FTIR data confirmed the presence of Ni-O and Co-O bond formation. The particle size of NiO-Co_3O_4 nano-ceramic composites particles present in the range nanometer range. The SEM photograph confirmed the presence of nano sized grains in the sample. The EDAX data confirmed the presence of three elements (nickel, cobalt and oxygen) in the samples. The optical studies were carried out for NiO-Co_3O_4 nano-ceramic composites using UV and PL techniques of the. Photocatalytic activity studies carried out with NiO-Co_3O_4 (1.0:1.0) nano-ceramic composites in presence of organic dyes such as, rhodamine B and methyl orange dyes under UV light irradiation (for two hours) resulted in the degradation of 77% and 84% respectively. Therefore, NiO-Co_3O_4 nano-ceramic composites may be considered as potential candidates for the degradation of organic dyes present in water.

ACKNOWLEDGEMENTS

The authors are grateful to the DST Nano Mission, Govt. of India, New Delhi for its support. The authors are also thankful to the management of Karunya University for its support and encouragement to carry out this research work.

REFERENCES

Abu-Zied, B. M. (2008). Oxygen evolution over Ag/$Fe_xAl_{2-x}O_3$ (0.0 d" x d" 2.0) catalysts via N_2O and H_2O_2 decomposition. Applied Catalysis A: General, **334,** 234-242.

Ai, L. H. and Jiang, J. (2009). Rapid synthesis of nanocrystalline Co_3O_4 by a microwave-assisted combustion method. Powder Technology, **195,** 11-14.

Amaral, P. F. F., Fernandes, D. L. A., Tavares, A. P. M., Xavier, A. B. M. R., Cammarota, M. C., Coutinho, J. A. P. and Coelho, M. A. Z. (2004). Decolorization of Dyes from textile wastewater by Trametes versicolor. Environmental Technology, **25,** 1313-1320.

Asiri, A. M., Al-Amoudi, M. S., Al-Talhi, T. A. and Al-Talhi, A. D. (2011). Photodegradation of Rhodamine 6G and phenol red by nanosized TiO_2 under solar irradiation. Journal of Saudi Chemical Society, **15,** 121-128.

Asokan, K., Park, J. Y., Choi, S. W. and Kim, S. S. (2010). Nanocomposite ZnO–SnO_2 nanofibers synthesized by electrospinning method. Nanoscale Research Letters, **5,** 747-752.

Bandara, J. and Yasomance, J. P. (2007). P-type oxide semiconductors as hole collectors in dye sensitized solid-state solar cells. Semiconductor Science and Technology, **22,** 20-24.

Beach, E. R., Shqaue, K. R., Brown, S. E., Rozesveld, S.J. and Morris, P.A. (2009). Solvothermal synthesis of crystalline nickel oxide nanoparticles. Materials Chemistry and Physics**, 115,** 373-379.

Chen, D. L. and Gao, L. (2005). A new and facile route to ultrafine nanowires, super thin flakes and uniform nanodisks of nickel hydroxide. Chemical Physics Letters, **405,** 159-164.

Chen, X. Y., Chen, J. W., Qiao, X. L., Wang, D. and Cai, X. (2008). Performance of nano-Co_3O_4/peroxymonosulfate system: Kinetics and mechanism study using Acid Orange 7 as a model compound. Applied Catalysis B: Environmental, **80,** 116-121.

Co, A. C., Liu, J., Serebrennikova, I., Abel, C. M. and Birss, V. I. (2005). Structural and Electrochemical Studies of Co oxide Films Formed by the Sol-Gel Technique. Journal of Materials **Science, 40,** 4039-4052.

Devi, B. S. R., Raveendran, R. and Vaidyan, A. V. (2007). Synthesis and characterization of Mn^{2+} doped ZnS Nanoparticles. Pramana - Journal of Physics, **68,** 679-687.

Gao, J., Luan, X., Wang, J., Wang, B., Li, K., Li, Y., Kang, P. and Han, G. (2011). Preparation of Er3:$YAlO_3$/Fe-doped TiO_2-ZnO and its application in photocatalytic degradation of dyes under solar light irradiation. Desalination, **268,** 68-75.

Gnanachari, S. V., Bhat, R., Deshpande, R. and Venkataraman, A. (2012). Synthesis and characterization of nickel oxide nanoparticles by self-propagating low temperature combustion method. Recent Research in Science and Technology, **4,** 50-53.

Hameed, A., Montini, T., Gombaca, V. and Fornasiero, P. (2009). Photocatalytic decolourization of dyes on NiO–ZnO nanocomposites. Photochemical and Photobiological Sciences, **8,** 677-682.

Han, D. Y., Yang, H. Y., Shen, C. B., Zhou X. and Wang, F. H. (2004). Synthesis and size control of NiO nanoparticles by water in oil microemulsion. Powder Technology, **147,** 113-116.

Hongve, D. and Akesson, G. (1996). Spectrophotometric determination of water colour in hazen units. Water Research, **30,** 2771-2775.

Irwin, M. D., Buchholz, D. B., Hains, A. W., Chang, R. P. H. and Marks, T. J. (2008). P-type semiconducting nickel oxide as an efficiency enhancing anode interfacial layer in polymer build hetero junction solar cells. Proceedings of the National Academy of Sciences, **105,** 2783-2787.

Kalu, E. E., Nwoga, T. T., Srinivasan, V. and Weidner, J. W. (2001). Cyclic voltammetric studies of the effects of time and temperature on the capacitance of electrochemically deposited nickel hydroxide. Journal of Power Sources, **92,** 163-167.

Kanjwal, M. A., Barakat, N. A. M., Sheikh, F. A., Park, S. J. and Kim, H. Y. (2010). Photocatalytic activity of ZnO-TiO_2 hierarchical nanostructure prepared by combined electrospinning and hydrothermal techniques. Macromolecular Research**, 18**, 233-240.

Keller, V. and Garin, F. (2003). Photocatalytic behavior of a new composite and oxides ternary system: WO_3/$SiCeTiO_2$ effect of the coupling of semiconductors in photocatalytic oxidation of methylethylketone in the gas phase. Catalysis Communications, **4,** 377-383.

Kim, S. G., Yoon, S. P., Han, J., Nam, S. W., Lim, T. H., Oh, I. H. and Hong, S. A. (2004). A study on the chemical stability and electrode performance of modified NiO cathodes for molten carbonate fuel cells. Electrochimica Acta, **49,** 3081-3089.

Lahiri, J. and Batzill, M. (2008). Surface functionalization of ZnO photocatalysts with monolayer ZnS. Journal of Physical Chemistry C, **112,** 4304-4307.

Lee, K. D. (2001). Influence of film thickness on the chemical stability of electrochromic tungsten oxide film. Journal of the Korean Physical Society, **38,** 33-37.

Li, W. Y., Xu, L. N. and Chen, J. (2005). Co_3O_4 Nanomaterials in Lithium-Ion Batteries and Gas Sensors. Advanced Functiona**l** Materials, **15,** 851-857.

Lou, X. W., Deng, D., Lee, J. Y., Feng, J. and Archer, L. A. (2008). Self-Supported Formation of Needlelike Co_3O_4 Nanotubes and Their Application as Lithium-Ion Battery Electrode. Advanced Materials, **20,** 258-262.

Mohamed Jaffer Sadiq, M. and Samson Nesaraj. A. (2013). Effect of surfactants in the synthesis of NiO nanoparticles by colloidal thermal assisted reflux condensation method. Journal of New Technology and Materials, **3,** 14-28.

Morsy, S. M. I., Shaban, S. A., Ibrahim, A. M. and Selim, M. M. (2009). Characterization of cobalt oxide nanocatalysts prepared by microemulsion with different surfactants, reduction by hydrazine and mechanochemical method. Journal of Alloys and Compounds**, 486,** 83-87.

Na, D. M., Satyanarayana, L., Choi, G. P. and Shin, Y. J. (2005). Surface morphology and sensing property of NiO–

WO_3 thin films prepared by thermal evaporation. Sensors, **5,** 519-528.

Nam, K. W. and Kim, K. B. (2002). A study of the preparation of NiO(x) electrode via electrochemical route for supercapacitor applications and their charge storage mechanism. Journal of Electrochemical Society, **149,** A346-A354.

Nethravathi, C., Sen, S., Ravishankar, N., Rajamathi, M., Pietzonka, C. and Harbrecht, B. (2005). Ferrimagnetic Nanogranular Co_3O_4 through Solvothermal Decomposition of Colloidally Dispersed Monolayers of α-Cobalt Hydroxide. Journal of Physical Chemistry B, **109,** 11468-11472.

Parada, C. and Moran, E. (2006). Microwave assisted synthesis and magnetic study of nano sized Ni/NiO materials. Chemistry of Materials, **18,** 2719-2725.

Park, C. and Keane, M. A. (2003). Catalyst support effects: gas-phase hydrogenation of phenol over palladium. Journal of Colloid and Interface Science**, 266,** 183-194.

Park, J. Y., Ahn, K. S., Nah, Y. C. and Shim, H. S. (2004). Electrochemical and electrochromic properties of Ni oxide thin films prepared by a sol gel method. Journal of **Sol-Gel Science** and **Technology, 31,** 323-328.

Pejova, B., Isahi, A., Najdoski, M. and Grozdanov, I. (2001). Fabrication and characterization of nanocrystalline cobalt oxide thin films. Materials Research Bulletin, **36,** 161-170.

Puspharajah, P., Radhakrishna, S. and Arof, A. K. (1997). Transparent conducting lithium doped nickel oxide thin films by spray pyrolysis technique. Journal of Materials Science, **32,** 3001-3006.

Rao, C. N. R. (1963). Chemical Applications of Infrared Spectroscopy, Academic Press, NewYork and London.

Romana, C. K. and Peter, B. (2006). Sol–Gel prepared NiO thin films for electrochromic applications. **Acta Chimica Slovenica, 53,** 136-147.

Sapra, S. and Sarma, D. D. (2005). Simultaneous control of nanocrystal size and nanocrystal - nanocrystal separation in CdS nanocrystal assembly. Pramana - Journalof physics, **65,** 565-570.

Sasi, B. and Gopchandran, K. G. (2007). Nanostructured mesoporous nickel oxide thin films. Nanotechnology, **18,** 115613-115621.

Sasikala, R., Shirole, A., Sudarsan, V., Sakuntala, T., Sudakar, C. and Naik, R. (2009). Highly dispersed phase of SnO_2 on TiO_2 nanoparticles synthesized by polyol-mediated route: photocatalytic activity for hydrogen generation. International Journal of Hydrogen Energy, **34,** 3621-3630.

Schneider, J. J. (2001). Synthesis of ZnO nanocrystals with cone, hexagonal cone, and rod shapes via non-hydrolytic ester elimination Sol–Gel reactions. Advanced Materials, **13,** 529-533.

Singhal, Achary, S., Tyagi, A., Manna, P. and Yusuf, S. (2008). Colloidal Fe-doped ZnO nanocrystals: Facile low temperature synthesis, characterization and properties. Materials Science and Engineering B, **153**, 47-52.

So, W. W., Kin, K. J. and Moon, S. J. (2004). Photo-production of hydrogen over $CdSe/TiO_2$ nanocomposite particulate films treated with $TiCl_4$. International Journal of Hydrogen Energy, **29,** 229-234.

Sun, L., Li, H., Ren, L. and Hu, C. (2009). Synthesis of Co_3O_4 nanostructures using a solvothermal approach. Solid State Sciences, **11,** 108-112.

Taniguchi, Fujioka, N., Ikoma, M. and Ohta, A. (2001). A development of nickel/metal-hydride batteries for EVs and HEVs. Journal of Power Sources**, 100,** 117-124.

Teo, J. J., Chang, Y. and Zeng, H. C. (2006). Fabrications of Hollow Nanocubes of Cu_2O and Cu via Reductive Self-Assembly of CuO Nanocrystals. Langmuir, **22,** 7369-7377.

Varghese, B., Zhang, Y., Dai, L., Tan, V. B. C., Lim, C. T. and Sow, C. H. (2008). Structure, Mechanical Property of Individual Cobalt Oxide Nanowires. Nano Letters **8,** 3226-3232.

Venkatnarayan, R., Kanniah V. and Dhathathreyan, A. (2006). Tuning size and catalytic activity of nano-clusters of cobalt oxide. Journal of Chemical Sciences, **118,** 179-184.

Wang, G., Shen, X., Horvat, J., Wang, B., Liu, H., Wexler, D. and Yao, J. (2009). HydrothermalSynthesis and Optical, Magnetic, and Supercapacitance Properties of Nanoporous Cobalt Oxide Nanorods. The Journal of Physical Chemistry C, **113,** 4357-4361.

Wang, Y., Zhu, J., Yang, X., Lu, L. and Wang, X. (2005). Preparation of NiO nanoparticles and their catalytic activity in the thermal decomposition of ammonium perchlorate. Thermochimica Acta, **437,** 106-109.

Wang, Z., Huang, B., Dai, Y., Qin, X., Zhang, X., Wang, P., Liu, H. and Yu, J. (2009). Highly photocatalytic ZnO/In_2O_3 heteronanostructures synthesized by a coprecipitation method. The Journal of Physical Chemistry C, **113,** 4612-4617.

Warang, T., Patel, N., Santini, A., Bazzanella, N., Kale, A. and Miotello, A. (2012). Pulsed laser deposition of Co_3O_4 nanoparticles assembled coating: Role of substrate temperature to tailor disordered to crystalline phase and related photocatalytic activity in degradation of methylene blue. Applied Catalysis A: General, **423,** 21-27.

Xin, X., Lu, Z., Zhou, B., Huang, X., Zhu, R., Sha, X., Zhang, Y. and Su, W. (2007). Effect of synthesis conditions on the performance of weakly agglomerated nanocrysalline NiO. Journal of Alloys and Compounds, **427,** 251-255.

Xing, W., Li, F., Yan, Z. and Lu, G. Q. (2004). Synthesis and electrochemical properties of mesoporous nickel oxide. Journal of Power Sources, **134,** 324-330.

Xu, S. P. and Sun, D. D. (2009). Significant improvement of photocatalytic hydrogen generation rate over TiO_2 with deposited CuO. International Journal of Hydrogen Energy, **34,** 6096-6104.

Xu, Z. P. and Zeng, H. C. (1998). Thermal evolution of cobalt hydroxides: a comparative study of their various structural phases. Journal of Materials Chemistry, **8,** 2499-2506.

Yan, J. H., Zhu, Y. R., Tang, Y. G. and Zheng. S. Q. (2009). Nitrogen-doped $SrTiO_3/TiO_2$ composite photocatalysts for hydrogen production under visible light irradiation. Journal of Alloys and Compounds**, 472,** 429-433.

Yang, H. Y., Yu, S. F., Lau, S. P., Zhang, X., Sun, D. D. and Jun, G. (2009). Direct growth of ZnO nanocrystals onto the surface of porous TiO_2 nanotube arrays for highly efficient and recyclable photocatalysts. Small, **5,** 2260-2264.

Yang, Q. J., Choi, H., Chen, Y. J. and Dionysiou, D. D. (2008). Heterogeneous activation of peroxy mono sulfate by supported cobalt catalysts for the degradation of 2,4-dichlorophenol in water: The effect of support, cobalt precursor, and UV radiation. Applied Catalysis B: Environmental, **77,** 300-307.

Yamamoto, H., Tanaka, S., Naito, T. and Hirao, K. (2002). Nonlinear change of refractive index of Co_3O_4 thin films induced by semiconductor laser (lambda=405 nm) irradiation**.** Applied Physics Letters, **81,** 999-1001.

Yu, X. D., Wu, Q. Y., Jiang, S. C. and Guo, Y. H. (2006). Nanoscale ZnS/TiO_2 composites: preparation, characterization and visible-light photocatalytic activity. Materials Characterization, **57,** 333-341.

Zav'yalova, U., Scholz, P. and Ondruschka, B. (2007). Influence of cobalt precursor and fuels on the performance of combustion synthesized $Co_3O_4/\gamma\text{-}Al_2O_3$ catalysts for total oxidation of methane. Applied Catalysis A: General, **323,** 226-233.

Zhang, Y., Liu, Y., Fu, S., Guo, F. and Qian, Y. (2007). Morphology-controlled synthesis of Co_3O_4 crystals by soft chemical method. Materials Chemistry and Physics, **104,** 166-171.